Chapter 2
Solar Radiation Measurements

2.1 Solar Radiation Components at the Ground Level

In a point at the top of Earth's atmosphere, the beam of nearly parallel incident sunrays is referred to as extraterrestrial radiation (ETR). ETR fluctuates about 6.9 % during a year (from 1412.0 Wm^{-2} in January to 1321.0 Wm^{-2} in July) due to the Earth's varying distance from the Sun. Figure 2.1 shows the spectral distribution of ETR at the mean Sun–Earth distance. The graph is plotted at low resolution with data from Gueymard and Myers (2008), which is detailed enough for many engineering applications, like forecasting of PV plants output. The extraterrestrial spectrum is also available online (NREL 2012), along with other reference radiation spectra. The integration of the extraterrestrial spectrum over all wavelengths defines the solar constant G_{SC}. Thus, G_{SC} represents the flux density of incoming solar radiation on a unitary surface perpendicular to the rays at the mean Sun–Earth distance. Since the Sun radiance varies to some extent over short and long periods (Fröhlich 1991), the solar constant does not remain steady over time. There is a variation of about $\pm$ 1 Wm^{-2} around the mean solar constant during a typical Sun cycle of 11 years (Gueymard and Myers 2008). Based on data collected over 25 years from terrestrial to space observations, the actual best estimate of the average solar constant is $G_{SC} = 1366.1$ Wm^{-2} (Gueymard 2004).

When the solar radiation flux passes through the Earth's atmosphere, its spectral distribution is modified by absorption and scattering processes. The complex effect experienced by solar radiation flux spectral distribution when transiting the Earth's atmosphere is also illustrated in Fig. 2.1, which displays the AM1.5G global spectrum defined by the Commision Internationale de l'Eclairage (CIE) and the American Society for Testing and Materials (ASTM) for testing the terrestrial solar cells. The standard assumes the following: the receiving surface is tilted 37° toward the equator, the solar zenith angle is 48°19', the total ozone column content is 0.34 cm atm, the Ångstrom turbidity coefficient at wavelength 0.5 μm is 0.084 and the water vapor column content is 1.42 g cm^{-2}. The Air Mass (AM)

M. Paulescu et al., *Weather Modeling and Forecasting of PV Systems Operation*, Green Energy and Technology, DOI: 10.1007/978-1-4471-4649-0_2,

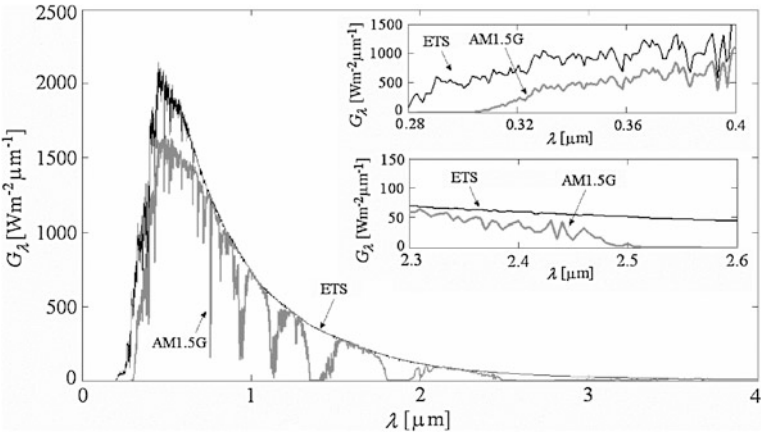

Fig. 2.1 Extraterrestrial solar spectrum (*ETS*) and terrestrial standard solar spectrum AM1.5G. Details of ultraviolet and infrared spectral domains are presented inset. G_λ is the extraterrestrial spectral flux density and λ is the photon wavelength

(see Chap. 5 for details), if approximated by the inverse of the cosine of the zenith angle, is $1/\cos(48°19') = 1.5$.

As a result of its passage through the atmosphere, the ETR is separated into different components. The beam component of solar radiation is that part of ETR which directly reaches Earth's surface. Scattering of the ETR in the atmosphere generates the diffuse component. A part of the solar radiation that is reflected by the ground may also be present in the total solar radiation. More precisely, the following quantities associated to solar radiation are commonly measured:

Direct beam irradiance (G_n) is the energy flux density (units: W/m^2) of the solar radiation incoming from the solid angle subtended by the Sun's disk on a unitary surface perpendicular to the rays.

Direct horizontal irradiance (G_b) differs from the direct beam irradiance in that it is measured on a flat horizontal plane. Lambert's cosine law states that the energy flux density on a plane surface is directly proportional to the cosine of the incidence angle. Since the incidence angle of the solar beam striking the horizontal ground is equal to sun the zenith angle θ_z (Fig. 2.2), then:

$$G_b = G_n \cos\theta_z \tag{2.1}$$

Diffuse irradiance (G_d) represents the energy flux density of the solar radiation incoming from the entire sky dome on a horizontal surface, excluding the direct beam coming from the Sun's disk.

Global irradiance (G) is the sum of the direct horizontal and diffuse components, given as:

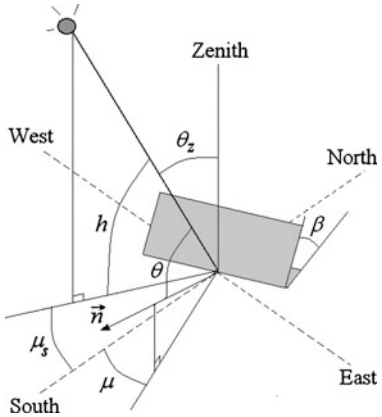

Fig. 2.2 Angles describing the position of the sun: θ_z—zenith angle; h—elevation angle, μ_s—azimuth angle. Angles describing the position of the surface: β—slope angle, μ—surface azimuth angle. The incidence angle θ is the angle between the sun direction and the surface's normal $\vec{n}$

$$G = G_b + G_d = G_n \cos\theta_z + G_d \tag{2.2}$$

The term "global" is associated to the fact that the solar radiation is received from the entire 2π solid angles of the sky vault.

The total irradiance (G_t) received by a surface tilted with an angle β in respect to the horizontal plane (Fig. 2.2) is the sum of beam flux density, diffuse flux density, and the additional flux density G_r of the solar radiation reflected from the ground, respectively. Usage of Eq. (2.2) yields:

$$G_t = G_n \cos\theta + R_d G_d + G_r \tag{2.3}$$

where θ is the incidence angle (i.e., the angle between the sun direction and the normal to the surface (Fig. 2.2), R_d is the conversion coefficient taking into account the sky view factor and G_r is the energy flux density of radiation reflected by the ground that is intercepted by the tilted surface. Models for estimating global solar irradiance on tilted surfaces differ generally in their treatment of R_d which is considered the main potential source of errors (see Chap. 5).

By summing up over a finite time period $\Delta t = t_2 - t_1$ one obtains the solar irradiation components:

$$H = \int_{t_1}^{t_2} G(t)dt \tag{2.4}$$

usually measured in J/m^2 or Wh/m^2. In Eq. (2.4), $G(t)$ stands for any of the above solar irradiance components, and consequently H refers to the corresponding solar irradiation component.

For proper characterization of the radiative regime the state of the sky should also be assessed. Two quantities are commonly used to describe the state of the sky. The most usual indicator is the total cloud cover amount C which represents the fraction of the celestial vault covered by clouds (estimated in tenths or oktas). The second quantity describing indirectly the state of the sky is the relative sunshine σ (also called sunshine fraction). It is defined as $\sigma \equiv s/S$, where S is the

length of a given time interval and s is the bright sunshine duration during that interval. State of the sky assessment is treated at large in Chap. 3.

2.2 Ground Measurements of Solar Radiation

Radiometry is the science of electromagnetic radiation measurement. The generic device is named radiometer.

Each of the quantities defined in Sect. 2.1 are measured with a specific device; for instance, the pyrheliometer that measures the direct beam irradiance and the pyranometer that measures the horizontal beam and diffuse irradiances. Details on both instruments will be presented in the following.

2.2.1 Solar Radiometers

Detection of the optical electromagnetic radiation is primarily performed by conversion of the beam's energy in electric signals that subsequently can be measured by conventional techniques. Due to their nearly constant spectral sensitivity for the whole solar spectral range, radiometers equipped with thermal sensors are widely used to measure broadband solar irradiance. Temperature fluctuations (the instruments are placed outdoor and their temperature may vary between −20 and 70 °C), wind, rain, and snow are factors that affect the measurements. The minimization of these perturbations is a difficult task in the engineering of solar radiometers.

Pyrheliometer

The pyrheliometer is a broadband instrument that measures the direct beam component G_n of solar radiation. Consequently, the instrument should be permanently pointed toward the Sun. A two-axis Sun tracking mechanism is most often used for this purpose. The detector is a multi-junction thermopile placed at the bottom of a collimating tube (Fig. 2.3a) provided with a quartz window to protect the instrument. The detector is coated with optical black paint (acting as a full absorber for solar energy in the wavelengths range 0.280–3 μm). Its temperature is compensated to minimize sensitivity of ambient temperature fluctuations. The pyrheliometer aperture angle is 5°. Consequently, radiation is received from the Sun and a limited circumsolar region, but all diffuse radiation from the rest of the sky is excluded. A readout device is used to give the instant value of the direct beam irradiance. Its scale is adapted to the sensitivity of the particular instrument in order to display the value in SI units, Wm^{-2}.

For illustration, a picture of a Hukseflux DR01 First Class pyrheliometer (Hukseflux 2012) is presented in Fig. 2.3b.

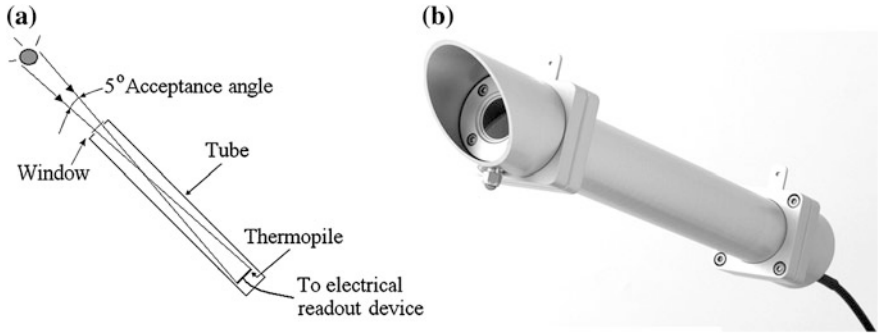

Fig. 2.3 **a** Schematic of a pyrheliometer. **b** Photo of Hukseflux DR01 first class pyrheliometer (Hukseflux 2012). (*Public license on Wikimedia commons*)

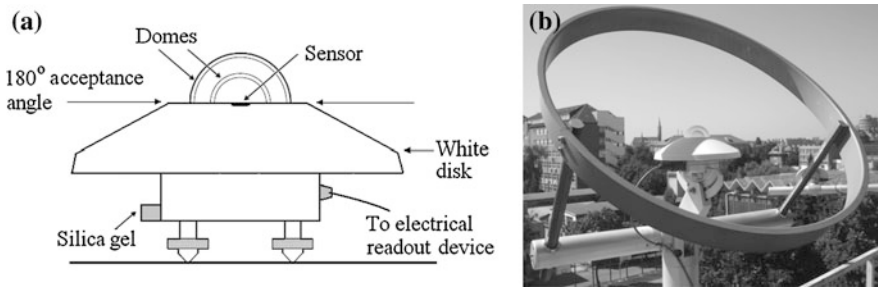

Fig. 2.4 **a** Schematic of a pyranometer. **b** First class pyranometer LPPYRA 12 (DeltaOHM 2012) equipped with shadow ring, mounted on the solar platform of the West University of Timisoara, Romania (SRMS 2012)

Pyranometer

Pyranometers are broadband instruments that measure global solar irradiance incoming from a 2π solid angle on a planar surface. A typical pyranometer is schematically represented in Fig. 2.4a. It consists of a white disk for limiting the acceptance angle to 180° and two concentric hemispherical transparent covers made of glass. The two domes shield the sensor from thermal convection, protect it against weather threat (rain, wind, and dust) and limit the spectral sensitivity of the instrument in the wavelength range 0.29–2.8 μm. A cartridge of silica gel inside the dome absorbs water vapor.

A pyranometer can be also used to measure the diffuse solar irradiance G_d, provided that the contribution of the direct beam component is eliminated. For this, a small shading disk can be mounted on an automated solar tracker to ensure that the pyranometer is continuously shaded. Alternatively, a shadow ring may prevent the direct component G_b from reaching the sensor whole day long (see Fig. 2.4b). Because the daily maximum Sun elevation angle changes day by day, it is necessary to change periodically (days lag) the height of the shadow ring.

Table 2.1 Characteristics of pyranometers, ISO 9060/1990 standard

ISO specification	Secondary standard	First class
WMO characteristics	High quality	Good quality
Response time (to reach 95 % of the final value)	<15 s	<30 s
Zero off-set response:		
—Response to 200 W/m^2 net radiation	7 Wm^{-2}	15 Wm^{-2}
—Response to 5 °C/h change in ambient temperature	±2 Wm^{-2}	±4 Wm^{-2}
Resolution	±1 Wm^{-2}	±5 Wm^{-2}
Stability (change in sensitivity per year)	±0.8 %	±1.5 %
Linearity (deviation from sensitivity at 500 Wm^{-2} over 100–1,000 Wm^{-2} irradiance range)	±0.5 %	±1 %
Directional response for beam radiation (error due when assuming that the normal incidence response at 1000 Wm^{-2} is valid for all directions)	±10 Wm^{-2}	±20 Wm^{-2}
Spectral selectivity (deviation of the product of spectral absorptance and transmittance, respectively, from the mean)		
ISO (0.35–1.5 μm)	±3 %	±5 %
WMO (0.3–3 μm)	±2 %	±5 %
Temperature response (maximum relative error due to any change of ambient temperature within a 50 °C interval)	±2 %	±4 %
Tilt response (percentage deviation from horizontal response when the tilt is changed from horizontal to vertical at 1,000 Wm^{-2})	±0.5 %	±2 %
Achievable uncertainty, 95 % confidence level		
WMO hourly totals	3 %	8 %
WMO daily totals	2 %	5 %

On the other hand, because the shadow ring also intercepts a part of the diffuse radiation, it is necessary to correct the measured values. The percentage of diffuse radiation intercepted by the shadow ring varies during the year with its position and atmospheric conditions (Siren 1987).

Self-calibrating absolute radiometers (Reda 1996) are used as primary standard, the other radiometers being calibrated against an absolute instrument. The uncertainty of the measured value depends on factors such as: resolution (the smallest change in the radiation quantity which can be detected by the instrument), nonlinearity of response (the change in sensitivity associated with incident irradiance level), deviation of the directional response (cosine response and azimuth response), time constant of the instrument (time to reach 95 % of the final value), changes in sensitivity due to changes of weather variables (such as temperature, humidity, pressure, and wind), long-term drifts of sensitivity (defined as the ratio of electrical output signal to the irradiance applied). All the above uncertainties should be known for a well-characterized instrument. Certain instruments perform better for particular climates, irradiances, and solar positions; therefore, the instruments should be selected according to their end use.

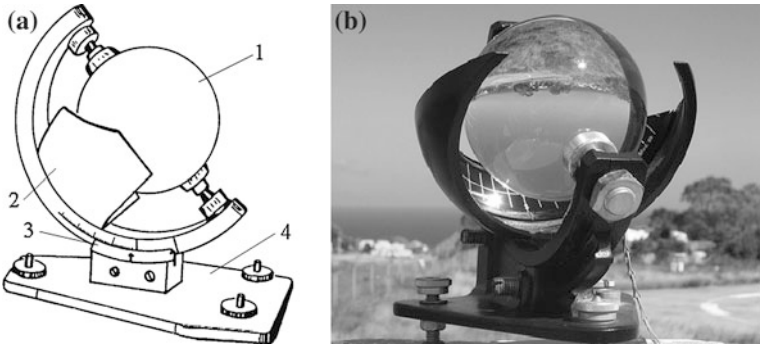

Fig. 2.5 **a** Schematic of Campbell-Stokes sunshine recorder. **b** Photo of a typical Campbell-Stokes sunshine recorder. (*Public license on Wikimedia commons*)

The accepted classification of pyranometers in respect to their quality is defined by the International Standard ISO 9060/1990 that is also adopted by the World Meteorological Organization (WMO 2008). ISO 9060 standard distinguishes three classes: the best is called (somewhat improperly) *secondary standard*, the second best is called *first class* and the third one—*second class*. Table 2.1 summarizes the characteristics of pyranometers of the first two levels of performance.

Sunshine duration measurement

According to (WMO 2008), sunshine duration in a given period is defined as the sum of the time intervals for which the direct solar irradiance exceeds the threshold of 120 Wm^{-2}. In practice, two methods are widely used for measuring sunshine duration—burning card method and pyranometric method—which will be briefly presented next.

Burning card method is based on the Campbell–Stokes sunshine recorder, which basic setup consists of a glass sphere mounted concentrically in a segment of a spherical bowl (Fig. 2.5). The support is adjustable so that the axis of the sphere may be inclined to the angle of the local latitude. The spherical bowl segment holds the recording card. The glass sphere focuses the direct beam solar radiation on to the card, burning a trace whenever the Sun is shining. The position and length of the trace indicate the starting time and duration of the sunshine interval. The errors of this recorder are mainly due to the dependence of burning initiation on card's temperature and humidity as well as to the overburning effect, especially in case of broken clouds (Kerr and Tabony 2004).

The pyranometric method implies measurement of global G and diffuse G_d solar irradiance; by subtraction, the direct beam solar irradiance is next derived, to be compared with the WMO threshold. Using the fundamental Eq. (2.2), the WMO sunshine criterion can be expressed as:

$$\xi(t) = \begin{cases} 1 & if \quad (G - G_d)/\cos\theta_z > 120\,\mathrm{W}/m^2 \\ 0 & otherwise \end{cases} \tag{2.5}$$

In Eq. (2.5) θ_z is the Sun zenith angle and ξ stands for the sunshine number (Badescu 2002), a Boolean variable stating whether the Sun is covered or not by clouds. Statistical properties of the sunshine number are investigated in Chap. 3 while methods to quantify the fluctuations of solar radiative regime by using the sunshine stability number are reported in Chap. 4.

The sunshine duration during a time interval Δt is obtained by multiplying Δt with the mean sunshine number $\bar{\xi}$ during Δt.

The errors in the pyranometric method stem from the errors of measuring global and diffuse solar irradiance, which are amplified at higher zenith angles (see Eq. 2.5). Choosing a high quality pyranometer is of primary importance to reduce the results uncertainty level. The usage of shading rings has as a consequence the undervaluation of the incident diffuse solar energy. Corrections are required to diminish this negative effect. Last but not least, the sampling frequency is important. At a higher measurement rate the sunshine duration can be evaluated more precise. At least one sample per minute is required to properly capture the fast changes of the solar radiative regime.

2.2.2 Surface Measurements

A comprehensive knowledge of the solar energy available in a location not only means its characterization by the total value, but also its temporal repartition, spectral distribution, and nature (direct or diffuse). Most countries have set up networks for measuring solar radiation but investments and maintenance costs for each site are not negligible. Thus, a national network often consists of relative small number of stations even in industrialized countries. Of course, the number of stations comprised in each network and measurement qualities varies from a network to another. Generally, global solar irradiation and sunshine duration are available on daily sums or monthly mean. Diffuse and direct components of solar irradiation, total cloud cover amount as well as data recorded on hourly basis are more rarely recorded. Only few stations around the world measure routinely the spectral distribution of solar radiation at the ground or the solar irradiance on tilted surfaces.

There is a sum of shortcomings associated with nowadays databases. The number of solar radiation stations is too small to achieve accurate global coverage. Consequently, interpolation and extrapolation of available data are used for estimation solar radiation in each point of the map. The errors in estimating solar irradiance in a given point increase with the distance from the closest station. The exact number of solar radiation stations measuring solar irradiance through the world is difficult to count, various sources giving different information. Even so, there are surely more than one thousand continental stations around the world that measure solar radiation. It was shown that daily solar irradiation measured at a station may be considered valid in an area of 30 km around (Cros and Wald 2003). Assuming that the 1,000 stations are equally distributed on land (146.94 millions of km^2), the probability of being in optimal vicinity of a station is less than 2 %.

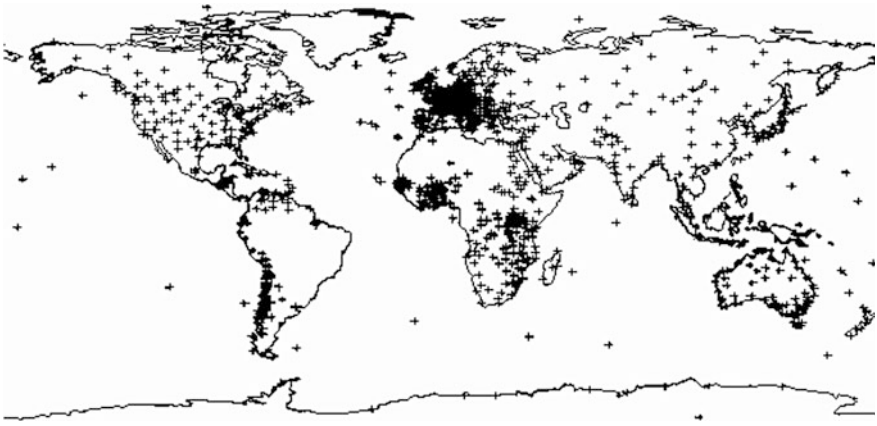

Fig. 2.6 Map of the stations contributing to the WRDC database (*Source* WRDC 2012b)

In other words, in 98 % of cases, the stations are too far to deliver accurate information to users. On the other hand, time characteristics of the data are often unsatisfactory. For example, beam solar irradiance, of vital interest in forecasting solar-thermal systems power output, is rarely available. Moreover, the databases store data in various formats and units using various time idioms. Thus, sometimes even data access and correct interpretation is a difficult task. It can be concluded that the solar radiation data from present databases are not matching many of the application requirements. There is enough room for efforts in integrating information systems to diminish the discrepancy between data availability and end user needs.

In the following, two large surface networks, World Radiation Data Center (WRDC) and Baseline Surface Radiation Network (BSRN) are summarized, while some national networks are only enumerated.

World Radiation Data Center (WRDC 2012a) collects data from the largest network for monitoring solar radiation, developed inside the WMO. WRDC is located at the Main Geophysical Observatory in St. Petersburg, Russia and serves as a central depository for solar radiation data collected at over one thousand measurement sites throughout the world (Fig. 2.6). The map presented in Fig. 2.6 shows that the spatial distribution of the stations is strongly heterogeneous through the world. The network is very dense in Western and Central Europe and Japan but there are large parts of the continents uncovered.

The system of collecting and archiving data is specified in the recommendations of the Meeting of Experts on the Future Activities of the WRDC (WMO 1983) and Resolution 6 (EC-XXXVI) of the World Meteorological Organization (WMO 1984). WRDC collects from WMO stations the results of measuring daily and hourly sums of radiation parameters with quality control check. WRDC performs a supplementary quality control and requests stations to confirm the data for total quality assurance. In addition to this basic information, WRDC receives

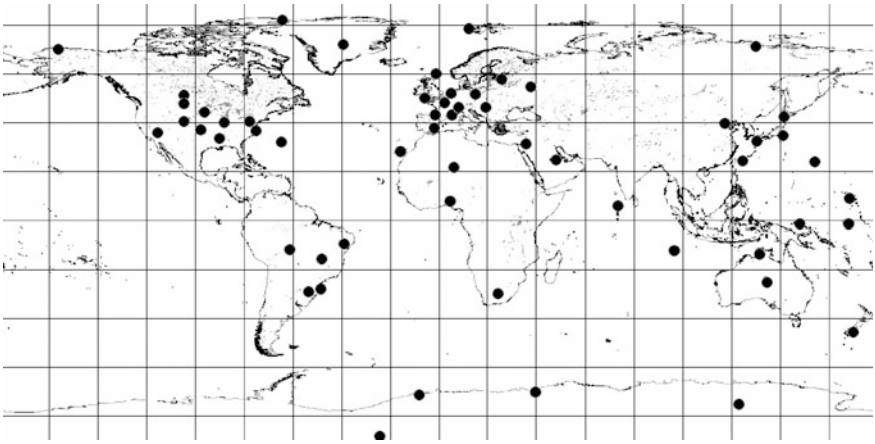

Fig. 2.7 Running and planning BSRN stations (BSRN 2012)

information on instruments and calibrations (supplementary information on this topic can be read in Ref. WRDC (2012b).

WRDC centrally collects, archives, and publishes radiometric data from the world to ensure the availability of these data for research by the international scientific community. WRDC archive contains mainly measurements of global solar irradiation, diffuse solar irradiation and sunshine duration in format of daily sums and monthly mean. Data collected from 1964 to 1993 are accessible online on the site of the US Department of Energy's, National Renewable Energy Laboratory (WRDC 2012b) and data collected from 1994 to present are accessible on the site of Main Geophysical Observatory, St. Petersburg, Russia (WRDC 2012a).

Baseline Surface Radiation Network (BSRN 2012). BSRN is a project of the Radiation Panel from the Global Energy and Water Cycle Experiment (GEWEX 2012) as part of the World Climate Research Program (WCRP 2012). The project is designated for detecting important changes in the Earth's radiation field at the Earth's surface which may be related to climate changes. Currently, about 40 stations located in contrasting climatic zones, covering a latitude range from 80°N to 90°S (see Fig. 2.7), are measuring solar and atmospheric radiation with instruments of the highest available accuracy and with high time resolution (1–3 min). The BSRN stations also contribute to the Global Atmospheric Watch (GAW 2012).

The solar radiation data are stored together with surface and upper-air meteorological observations in an integrated database. The BSRN database has been developed for storing high quality radiation data. It adds its own quality control process to that from the member organizations collecting data. The BSRN measurements are used to validate the radiation schemes in global climate models and satellite algorithms.

In addition to global networks there are also national networks which are repository for solar radiation data.

An important national solar radiation monitoring network has been developed by the US National Oceanic and Atmospheric Administration, namely NOAA's Surface Radiation (SURFRAD 2012). Independent measures of upwelling and downwelling solar and infrared radiation are the primary measurements; auxiliary observations include direct and diffuse solar irradiance, photosynthetically active radiation, UVB, and meteorological parameters. Quality controlled data are packed into daily files that are distributed almost in real time by anonymous FTP and HTTP protocols (SURFRAD 2012). Quality assurance built into the design and operation of the network and a good data quality control ensures that a continuous, high accuracy product is released. Another program is the US Department of Energy Atmospheric Radiation Measurement (ARM 2012) with the aim to increase the knowledge about the interaction between clouds and atmospheric radiative fluxes. From the observational perspective, the focus is on measuring the solar and thermal infrared radiative fluxes at Earth's surface and of all the atmospheric quantities that affect those fluxes. The Cooperative Network for Renewable Resource Measurements (CONFRRM 2012) is another important source of solar radiation data. CONFRRM is a joint effort between the US National Renewable Energy Laboratory and other agencies to conduct long-term solar radiation and wind measurements at selected locations in the United States. CONFRRM provides high quality data for determining site-specific resources, as well as data for the validation and testing of models to predict available resources based on meteorological or satellite data. Quality control and quality assurance occur before and during data collection and include procedures such as the proper selection and installation of instruments and data acquisition equipment, as well as regular maintenance and calibration. Collected data are also post processed, to check in a final quality assessment whether a data value is reasonable, too small, too large, or missing.

All European countries have established and maintain national networks for solar radiation measurements and contributing to WRDC database. The spatial density of stations in the national networks and their quality varies from a country to country. For example, in Spain, which is an important actor in the photovoltaic research and market, there are 52 stations currently contributing to WRDC. Taking into account that the surface of Spain is 504,030 km^2, the stations spatial density is roughly 1–10,000 km^2. In Eastern Europe, in Romania, the national meteorology network comprises 150 meteorological stations but less than 10 maintain a long-term global solar irradiation database and contribute to WRDC. The stations spatial density is 1–24,000 km^2, 2.5 times lower than in Spain.

In Europe, there are several integrated information systems, where databases are supplemented by post processing products like maps and software, available online or on CD-ROMs. Two examples follow.

Photovoltaic Geographical Information System (PVGIS 2012) is a research and demonstration instrument for geographical assessment of solar resource and solar systems in the context of distributed energy generation (Suri et al. 2005). The server, operated by the Joint Research Center of the European Commission, offers

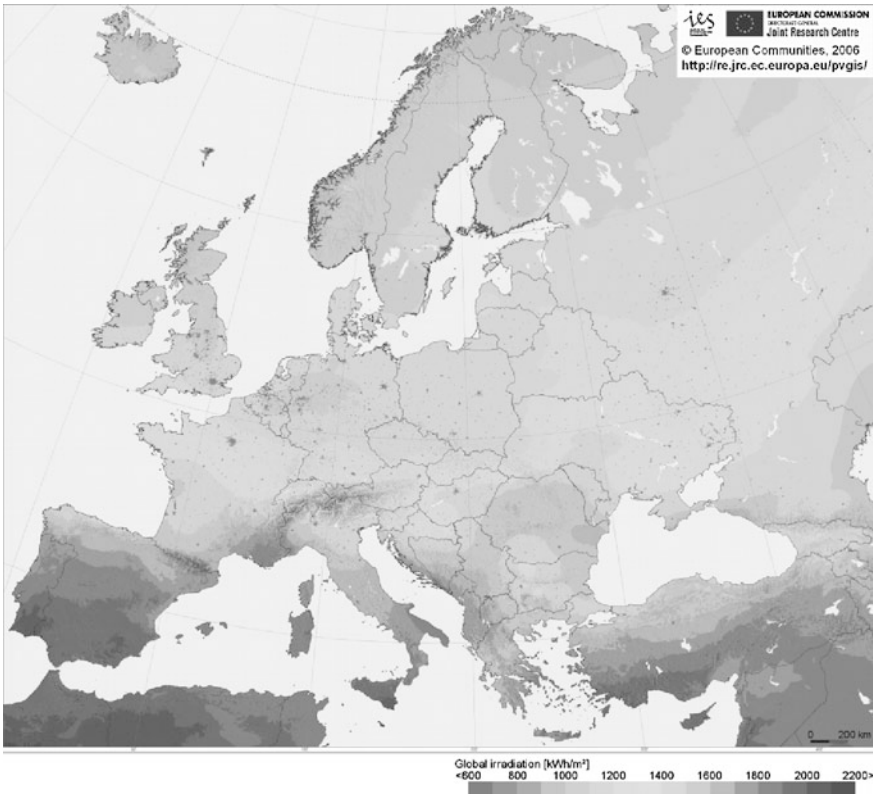

Fig. 2.8 Yearly global solar irradiation over Europe incident on optimally inclined (*equal to local latitude*) south-oriented surface (Suri et al. 2007)

map-based query of basic statistics of solar radiation, temperature, and the other data for two regions: Europe and Northern Africa. For Europe the database is based on an interpolation of ground station measurements (1 km grid, period 1981–1990). Figure 2.8 shows an example of European solar radiation map provided by the PVGIS. For the Mediterranean Basin and Africa the maps are developed by processing the HelioClim-1 database (2 km grid resolution, period 1985–2004).

METEONORM (METEONORM 2012) is a comprehensive climatologic database for solar energy applications combined with a synthetic weather generator. It contains a large database of ground station measurements collected from various sources (more than 8,300 are listed for the version 7). Two time periods of the measurements are available: (1) 1961–1990 and 1996–2005 for temperature, humidity, precipitation, and wind speed, and (2) 1961–1990 and 1981–2000 for radiation parameters. Enhanced satellite data are used to improve the estimations for areas with low density of weather stations. The METEONORM outputs are climatologic averages and derived products for any point on earth, estimated by

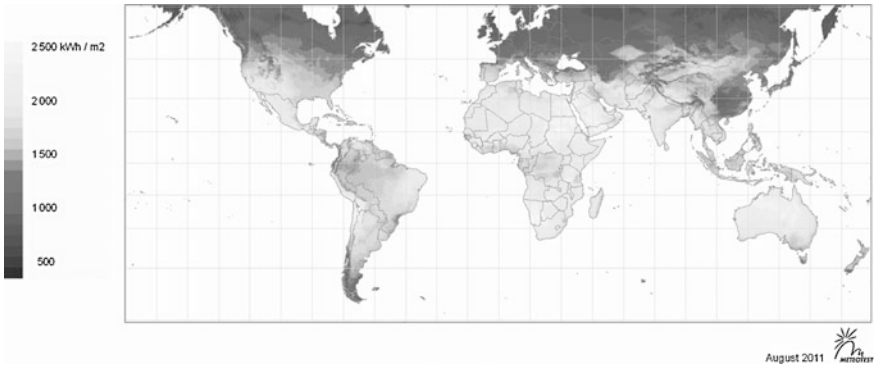

Fig. 2.9 Yearly global solar irradiation over the world, period 1996–2005, grid size 0.33° uncertainty 7 %. *Source* METEONORM (http://www.mwteonorm.com)

interpolation at very high resolution (0.1–1 km). A world map of yearly sum of daily global solar irradiation generated by the METEONORM software is presented in Fig. 2.9.

2.3 Solar Radiation Derived from Satellite Observation

In the previous section, we have seen that even if the availability of ground solar radiation data is on the rise, the spatial density of stations is still far too low. In order to fill the gaps in surface measured data, approaches based on satellite observation turn into a suitable alternative. In the last decades, a number of methods for estimating solar radiation from satellite data have been developed (e.g. Vonder Haar et al. 1973; Moser and Rachke 1984; Cano et al. 1986; Nunez 1993; Zelenka et al. 1999; Perez et al. 2002; Schillings et al. 2004; Rigollier et al. 2004; Janjai et al. 2005; Martins et al. 2007; Janjai 2010).

Most of the methods for deriving solar radiation from satellite observations employ meteorological geostationary satellite images. The geostationary satellites, orbiting at about 36,000 km, can offer a temporal resolution of up to 15 min and a spatial resolution of up to 1 km. The meteorological satellites collect images over a large area and with high time resolution allowing identification and forecasting the clouds evolution. This information is further processed, leading to the prediction of spatial variability of solar radiation at the ground level. Compared to ground measurements, satellite-derived hourly irradiation has been shown to be the most accurate option for locations that are further away with more than 25 km from a ground station (Zelenka et al. 1999). Thus, processing data collected by satellites can be a viable solution for forecasting solar radiation at the ground, aiming to proper operate the power grid.

A brief review of the satellite-based approaches for deriving solar radiation followed by a survey of available databases is presented next.

2.3.1 Satellite Based Models for Deriving Solar Radiation

The equation that governs the satellite-based models is derived from the interaction of ETR with the Earth-atmosphere system. This way, a part of ETR (G_{ext}) is reflected (G_r), other part is absorbed (G_a), and the remaining (G_g) is absorbed by the ground. Enclosed in brackets is the notation for the corresponding energy flux density. The energy conservation gives:

$$G_{\text{ext}} = G_r + G_a + G_g \tag{2.6}$$

Expressing the energy absorbed by the ground as a function of global solar irradiance $G_g = (1 - \rho)G$, where ρ is the surface albedo, Eq. (2.6) becomes:

$$G = \frac{1}{1-\rho}(G_{\text{ext}} - G_r - G_a) \tag{2.7}$$

Equation (2.7) represents the basis of all models developed for retrieving solar irradiance from satellite images. In Eq. (2.7), G_{ext} is well defined by astronomical equations (see Chap. 5) and G_r is measured by the satellite radiometer. The methods for estimating ground data differ by the way in which G_a and ρ are estimated.

Three models are summarized below: Heliosat model (HelioClim 2012), Operational Model (Perez et al. 2002), and Janjai model (Janjai et al. 2005).

Heliosat method (HelioClim 2012) converts images acquired by meteorological geostationary satellites, such as Meteosat (Europe), GOES (USA), or GMS (Japan), into data and maps of solar radiation received at ground level.

The development of Heliosat method is an ongoing effort of the Center for Energy and Processes, Ecole des Mines de Paris/Armines, France (CEP 2012).

The original model proposed by Cano et al. (1986) was improved through different versions. The basic idea is that the cloud cover amount over a given area statistically determines the global solar irradiance for that area. Thus, the processing takes two steps. A cloud cover index is derived for each pixel of the original satellite image and subsequently used in a second step for estimation of the global solar irradiance.

The cloud cover index is a basic concept in retrieving solar irradiance from satellite images. This parameter has been defined in Cano et al. (1986) as:

$$n = \frac{\rho - \rho_g}{\rho_c - \rho_g} \tag{2.8}$$

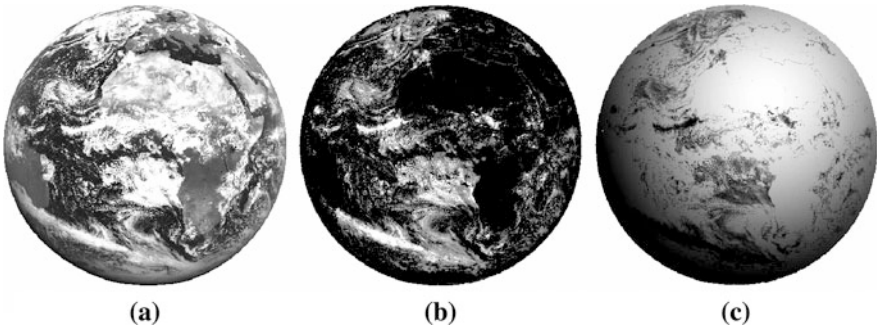

Fig. 2.10 Illustration of the processed images by using the Helisat-2 model (http://www.helioclim.org/heliosat/): **a** Raw meteosat data (August 1, 1992, 11h30). **b** Derived cloud cover index. **c** Derived hourly solar global irradiation. *Image courtesy* Lucien Wald

where ρ is the albedo measured by the satellite, ρ_c is the cloud albedo and ρ_g is the ground albedo. The cloud cover index ranges from 0 to 1 and may be interpreted as the percentage of the cloud cover amount per pixel.

Heliosat-1 model consists basically in a linear correlation of cloud cover index n and instantaneous clearness index k_t (Diabate et al. 1988):

$$k_t = an + b \tag{2.9}$$

were a and b are empirical parameters.

Heliosat-2 version (Rigollier et al. 2004) is dealing with atmospheric extinction and cloud extinction separately. The clear sky solar irradiance is calculated with the ESRA model (Rigollier et al. 2000), briefly summarized in Chap. 5 of this book. It uses at input only the Linke turbidity factor, a parameter that signifies the number of clear and dry atmospheres required to yield the observed extinction. Inputs to the method Heliosat-2 are not numerical counts of the satellite image, like in Heliosat-1. These counts are calibrated and thus converted into radiances. The Heliosat-1 construction of cloud cover index has been in principle preserved in the updated version Heliosat 2. Figure 2.10 presents an example of the processed Earth images by using the Helioclim-2 method.

Heliodat-3 version uses a new type of correlation scheme based on a radiative transfer code (Mueller et al. 2004), which makes use at input of atmospheric parameter information (clouds, ozone, and water vapor) retrieved from the Second Generation of Meteosat satellites databases (spatial resolution 1/3 km; temporal resolution 15 min; spectral channels 12).

Operational Model (Perez et al. 2002) is also a development of the Cano model. It has been elaborated at the Atmospheric Sciences Research Center (ASRC 2012) of the University of Albany, USA and applied to GOES satellite images. Cloud cover index is used to modulate the global solar irradiance estimated under clear sky using atmospheric turbidity as entry. The estimation of clear sky global solar irradiance G_0 is based on the Kasten (1980) model with some modifications to

exploit an atmospheric turbidity coefficient formulation, which removes the dependence on solar geometry (Ineichen and Perez 2002). The model equation is:

$$G_0 = c_1(z)G_{\text{ext}} \exp[-mc_2(z)(c_3(z) + c_4(z)(T_L - 1))] \exp\left[0.01m^{1.8}\right] \cos\theta_z \quad (2.10)$$

where $c_1(z) = 0.0509z + 0.868$, $c_2(z) = 0.0392z + 0.0387$, $c_3(z) = \exp(-z/8)$ and $c_4(z) = \exp(-z/1.25)$. In Eq. (2.10), z is the site altitude (in km), θ_z is the zenith angle, m is the altitude-corrected AM and T_L is the Linke turbidity factor. Details on the computations of these quantities are given in Chap. 5.

For each area (e.g. pixel), the global hourly irradiance is estimated by adapting G_0 to the actual cloud cover amount by means of cloud index:

$$G = G_0(0.0001\,G_0 f(n) + 0.9)f(n) \quad (2.11)$$

where $f(n) = 2.36n^5 - 6.2n^4 + 6.22n^3 - 2.36n^2 - 0.58n + 1$.

The model can also exploit operationally available snow cover resource data, while deriving local ground specular reflectance characteristics from the stream of incoming satellite data.

The operation of the model on a geographic scale, either for the preparation of maps or site/time-specific time series requires some degree of logistics and information processing. This includes several layers of gridded information: (1) Raw satellite pixels obtained via direct processing of primary GOES satellite images. The achievable resolution of visible channel GOES image could approach 0.01°. (2) Terrain elevation. (3) Climatological Linke turbidity. (4) Snow cover (5) Specular correction factor.

Janjai model (Janjai et al. 2005) has been developed for mapping solar irradiation in a tropical environment. An improved variant has been reported in Janjai (2008) and is briefly summarized below. Apart from the previous models, the Janjai model does not focus on the calculation of solar irradiance for each hourly satellite image. It is motivated by the fact that the state of the sky may experience high fluctuation in this time interval (especially in the tropics). This implies serious limitations on the ability of satellites to map irradiance by using only several scan images. Instead, the regional cloud structure emerges after daily averaging. Thus, the proposed method is aimed to the calculation of long-term averages of daily radiation using long-term satellite data. All parameters involved in the satellite model are calculated on monthly average basis. The outcome of the calculation belongs to solar radiation climatology which is usually required for generating a map for solar energy applications.

In this model, the incident solar radiation which enters the earth's atmosphere is scattered back to the outer space by air molecules and clouds with the cloud atmospheric albedo ρ_A and by atmospheric aerosols having an albedo ρ_{aer}. The rest of the radiation continues to travel downward and is absorbed by ozone, mixed gases, water vapor, and aerosols with absorption coefficients α_O, α_g, α_w and α_{aer}, respectively. Upon reaching the surface, the radiation flux is reflected back by the ground with the albedo ρ_g. As it passes upward through the atmosphere, it is further depleted by aerosol scattering (ρ_{aer}) and aerosols absorption (α_{aer}) and

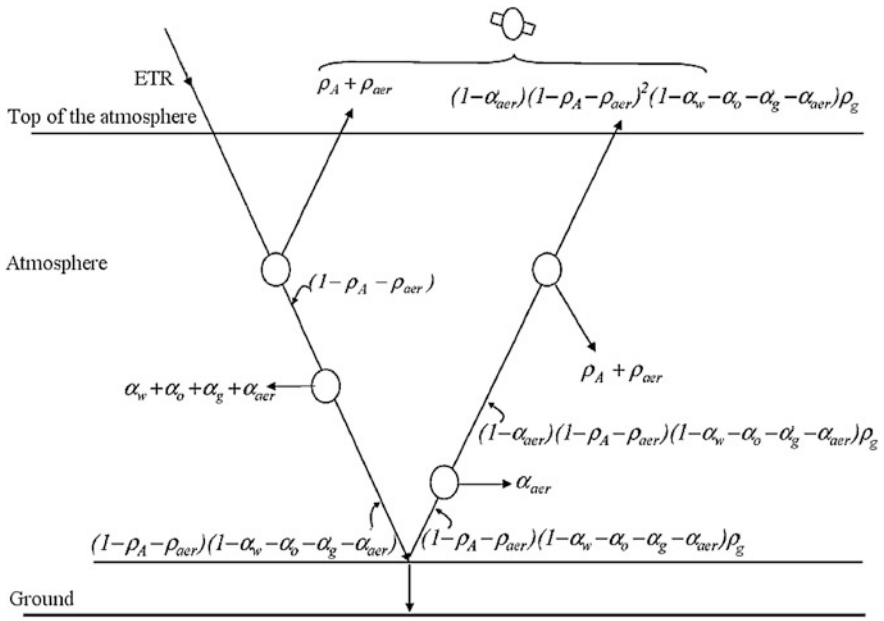

Fig. 2.11 Schematic diagram showing the radiation budget in the atmosphere as it is showing by the satellite in a spectral band. (ρ_A is the cloud—atmospheric albedo, ρ_{aer}. is the atmospheric aerosols albedo and ρ_g is the ground albedo. α_O, $\alpha_{g\alpha}$, α_w and α_{aer} stand for absorption coefficients of ozone, mixed gases, water vapor and aerosols, respectively. After Janjai (2008), with permission

cloud-atmospheric scattering ($\rho_A\rangle$. No further absorption due to water vapor, ozone, and gases is considered as it is assumed that the spectral irradiance in the absorption band of these atmospheric constituents has been absorbed completely during the downward travel of the solar flux. These processes are schematically shown in Fig. 2.11.

The albedo of the earth-atmosphere system detected by the satellite in a spectral band (e.g., 0.55–0.72 μm for GOES 9) can be written as:

$$\rho_{\text{EA}} = \rho_A + \rho_{\text{aer}} + (1 - \rho_A - \rho_{\text{aer}})^2\left(1 - \alpha_o - \alpha_w - \alpha_g - \alpha_{\text{aer}}\right)(1 - \alpha_{\text{aer}})\rho_g \tag{2.12}$$

This model employs satellite data to estimate cloud-atmospheric albedo in the satellite band, which is converted into a broadband cloud-atmospheric albedo using global radiation measured at ground stations. This broadband albedo and surface recorded supplementary data are used to map daily global radiation. The preparation of satellite data, the determination of the model coefficients, the conversion procedures, and a model accuracy assessment are detailed in Janjai (2008).

2.3.2 Online Available Databases

Solar radiation information from satellite data provided by web-based systems and databases are mainly solar radiation maps. Some websites also act as data servers. Four frequently accessed websites involving solar radiation derived from satellite images are reviewed in the following.

Satel-Light—European Database of Daylight and Solar Radiation (Satel-Light 2012) was probably one of the first web sites to provide solar radiation data. The Satel-Light project was funded by the European Union from 1996 to 1998. The methodology is based on the Heliosat model. Images produced by the Meteosat satellite every half hour are the only one source of information. Satel-Light service covers Europe and a small region of the North Africa. The information provided concerns solar irradiance and daylight statistical data in terms of monthly means of hourly and daily values from the period 1996 to 2000.

SoDa—The project Solar Data (SoDa 2012) is an effort to consolidate different databases through a web server containing solar radiation parameters and other relevant information: long-term time series of daily irradiation, climatic data and derived quantities, simulation of radiation under clear skies, and simulation of different solar power systems. The Quality Assessment benchmark of the SoDa database consists of weighing the estimated values against the corresponding ground station measurements. Data are disseminated by the SoDa website through the SoDa Service. A service or a resource can be a database (e.g., solar radiation database, temperature database), an algorithm that performs on data to create new information or an application that provides information that can be directly used in practice. The SoDa database is processed by MINES ParisTech—ARMINES (HelioClim 2012).

NASA Surface Meteorology and Solar Energy (SMSE 2012) is a large archive of over 200 satellite-derived meteorological and solar radiation parameters. The data are available on a 1° longitude by 1° latitude equal-angle grid covering the entire globe (64,800 regions). The data are generated using the GEOS 4 dataset, with a resolution of 1.25° longitude and 1° latitude. Interpolation is used to produce $1 \times 1°$ regions. The solar radiation data are generated using the Pinker and Laszlo (1992) algorithm. Cloud information is taken from the International Satellite Cloud Climatology Project DX dataset on an equal area grid with an effective 30×30 km pixel size. The output data are generated on a nested grid with a resolution of one degree latitude globally and longitudinal resolution ranging from 1° in the tropics to 120° at the poles. This is regridded to a 1° equal-angle grid (360 longitudes by 180 latitudes). The regridding method is done by replication wherein any grid region that is larger than $1 \times 1°$ is subdivided into $1 \times 1°$ regions, each taking the same value as the original.

Data quality control is carried out by comparison with ground measured data. Regression analysis of SMSE versus BSRN monthly averaged values of global solar irradiation for the time period July 1983 to June 2006 shows a relative root

mean square error of 10.25 % and the relative mean bias error of −0.01 % (SMSE 2012).

Data can be retrieved from the SMSE server (SMSE 2012), where they are organized in groups fitting various solar applications, e.g., sizing and pointing solar modules, solar cooking, tilted solar modules, cloud information, and so on.

The *Australian Bureau of Meteorology* (ABM 2012) maintains an online service (Climate Data Online), which provides historical data of daily global solar irradiation in a variety of formats (table, graphs). The data are derived from satellite images taken by the Geostationary Meteorological Satellite GMS-5, Geostationary Operational Environmental Satellite (GOES-9), and MTSAT-1R and MTSAT-2 satellites. The process of displaying the data uses the latitude and longitude of the Bureau's ground observation stations to retrieve the solar radiation values for a point within Australia. A basic site summary and topographic map of the area around the Bureau station is available online (ABM 2012).

2.4 Data Assessment Related to PV Power Forecasting

A PV plant project goes through two stages: (1) development and (2) PV plant exploitation. Different kinds of information on solar resource are needed in each stage.

In the development stage reliable solar radiation statistics are required for plant location, system design, and for feasibility study. In most cases, monthly averages values of solar irradiation or TMY—typical meteorological year (e.g. Janjai and Deeyai 2009) are enough. The overview made during this chapter on the existing databases of solar resource data shows that they contain adequate information for the development stage of a power plant. In most situations the data, either raw or completed by estimations, may convene the needs of users. Questions may arise on quality issues and uncertainty related to the methods of measurement and data processing, which varies from station to station and from a database to another. Even if the years after 2000 brought a real progress in data quality assurance, improvement is still needed. The fact that uncertainties in solar data can make the difference between profit and loss stresses the importance of the data quality issue.

In the exploitation stage of a power plant, forecasting the output power is required for proper operating the power grid. Moreover, real-time data flow is critical for optimizing supply/demand patterns in the power grid with multiple fluctuating sources, PV plants and/or wind farms. Thus, accurate forecasting of solar irradiance became a mandatory task. Depending on the time horizon, different forecasting methods are considered. In the shortest time domain ("Nowcasting", 0–3 h), numerical weather models perform badly: the forecast has to be based on extrapolations of real-time measurements. In the second time domain ("Short-Term Forecasting", 3–6 h), numerical weather models are coupled with post-processing modules in combination with real-time

measurements. In the third time domain ("Forecasting", 6–72 h or more), only the numerical weather model in combination with post-processing modules and satellite information are recommended (Lara-Fanego et al. 2012). For the reason that this book is mostly dedicated to nowcasting solar radiation and the topics are focused on statistical and artificial intelligence approaches, numerical weather prediction (NWP) models are acknowledged briefly in Sect. 2.5.

Existing surface databases are of little use to forecast solar irradiance since the information contained in them is far from real time. Consequently, it is optimal for each PV plant to have its own solar irradiance and meteorological parameters measuring station to provide the basis for time series forecasting. On the other hand, solar irradiance data retrieved from satellite images are of major importance in evaluating temporal and spatial changes of the solar resource, most important in regions with multiple and large PV capacities. Flow maps of the direct beam radiation occurring at the ground can be performed at a time resolution of 15 min.

2.5 Numerical Weather Prediction Models

NWP uses the current weather conditions as input into mathematical models describing the processes occurring in the atmosphere to predict the weather for a certain future period. Historically, NWP starts with the work of V. Bjerknes and L. F. Richardson in the beginning of the last century (Lynch 2008). The first operational forecast has been produced in 1954 by Carl-Gustav Rossby's group at the Swedish Meteorological and Hydrological Institute (Harper et al. 2007). The first successful climate model has been developed in 1956 by N. A. Phillips (Philips 1956; Cox 2002) while the first general circulation climate model has been developed about 1970 at NOAA Geophysical Fluid Dynamics Laboratory (NOAA 2008). Several limited area (regional) models have been proposed and implemented in the 1970 and 1980s (Shuman 1989). Starting in the 1990s, model ensemble forecasts have been used to extend NWP forecasting period (Molteni et al. 1996; Toth and Kalnay 1997).

A comprehensive overview of techniques used in numerical weather forecasting can be found in Coiffier and Sutcliffe (2012). This book presents a short history of NWP and their evolution followed by a step-by-step description of the various model equations and how to solve them numerically. This book outlines the main elements of a meteorological suite and the theory is illustrated throughout with practical examples.

2.5.1 NWP Categories

The NWP models may be classified in General Circulation Models (GCMs), which describe processes at global level, and regional or local models, whose application surface area is restricted. Local NWP models use atmospheric reanalyzes as initial and boundary conditions for the model run, which then realistically downscale (using physical equations) to a more accurate physical resolution. The NWP model that downscales reanalyzes data is termed a mesoscale model. Because the mesoscale models run over a smaller area than global scale models, the physics can include additional details. Therefore, given enough computing power, these models can be used to forecast various meteorological parameters over a wide area with high temporal and spatial resolution.

Among the most popular GCMs are Global Forecast System (GFS), ECMWF (a model developed by the European Center for Medium-Range Weather Forecasts), UKMO (developed by the United Kingdom Met Office) and GME (the model of Deutsche Wetterdienst) while among the regional/local models one may quote HRM (High Resolution Model), High-Resolution Limited Area Model (HIRLAM), WRF-Nonhydrostatic Mesoscale Model (WRF-NMM), WRF-ARW (Advanced Research WRF), The Unified Model and MM5 (Mesoscale Model) (Santos-Munoz et al. 2009; Isvoranu 2011). Generally, the local models are using boundary and initial conditions obtained by running GCMs. However, the local models may also be run by using boundary and initial conditions provided by the user.

WRF model has a wide range of physical parameterizations, which allow setting the model to better describe the physical processes based on model domain, resolution, location, and application (Ruiz-Arias et al. 2008).

Selection of NWP models is based on the following criteria: (1) performance; (2) cost; (3) popularity; (4) easy access to ground and satellite meteorological data to be used as boundary and initial conditions. European researchers prefer to use models such as HRM and HIRLAM while researchers in USA and Canada prefer WRF and MM5 (Grell et al. 1998). Most models developed in Europe are based on a semi-Lagrangean treatment of the primitive equations. North-American models are usually based on the Eulerian approach. Presently, all models allow both deterministic and probabilistic simulations (Isvoranu 2011).

The performance of diverse NWP models has been analyzed in several papers. For instance, results provided by WRF-NMM, UKMO, and GME have been compared in Santos-Munoz et al. (2009). Also, the models WRF and ECMWF have been analyzed in Matsangouras et al. (2011). These studies show a better performance for WRF model. There is, indeed, an increased popularity of this model in Europe (Isvoranu 2011).

Since individual weather prediction models have their specific strengths and weaknesses in certain weather situations, the results of several different models are usually compared with practice. Another approach is to use the same model, run it with different boundary conditions and compare the results (ensemble forecast). An important parameter is the forecast uncertainty which is derived by using

statistical methods or ensemble forecasts and still represents a challenging and complex task due to the chaotic nature of the weather. The output of the weather prediction models is then post-processed and improved with statistical combination of past and/or online measurement data. To achieve this goal, a number of statistical methods can be used to reduce the systematic forecast errors (e.g., model output statistics, Kalman filter, fuzzy logic, and neural network).

2.5.2 NWP for Renewable Energy Forecasting

Wind power forecasts have a high level of quality driven by the strong development of wind energy in countries like Germany, Denmark, or Spain. There exists already a number of providers of operational forecasts, but the forecast systems are mainly focusing on large wind park areas in flat terrain and mid-latitudes, though potential for wind energy production is also very high in mountainous/hilly areas and arctic conditions (e.g., in northern Scandinavia, the Alps, and in South-Eastern Europe). Unlike the wind power, solar yield forecast is still on an early state. The basic principles of solar power forecasts are more or less similar to wind power forecasts but other parameters need to be considered. There are mainly two different ways for solar electricity production: by solar-thermal power plants and by PV plants. The solar-thermal systems use the direct-normal solar irradiance to convert solar energy through focusing receivers into heat, which is then used to drive a thermodynamic cycle and thereby produce electricity. PV systems enable direct conversion of global horizontal irradiance into electricity through semiconductor devices.

Different approaches to forecast irradiance can be taken depending on the target forecasting time. For very short time forecasts (up to 6 h, nowcasting), approaches based on extrapolating the solar radiation field from cloud motion have been proposed (Heinemann et al. 2006). These forecasts are meant for solar field control in solar-thermal and PV plants. In addition, statistical techniques have been proposed for forecasting solar irradiance with up to 24 h (Mellit and Pavan 2010). NWP models are the basis of solar yield forecasts with up 48 h time horizon, the time range useful for grid integration and decision making in the energy market.

Evaluation studies on the MM5 mesoscale model reliability for estimating global solar irradiance were carried out by Zamora et al. (2005) in some locations in USA. Heinemann et al. (2006) evaluated the MM5 model global irradiance forecasts in Germany for lead time up to 48 h. Lorenz et al. (2009a) evaluated several NWP-based GHI forecasts in Europe. Overall, results showed relative RMSE values of about 40 % for Central Europe and about 30 % for Spain. Lorenz et al. (2009b) evaluated hourly global irradiance forecasts, based on ECMWF model, for power prediction of PV systems in Germany. They reported relative RMSE values of about 35 % for single stations for a 24 h horizon forecasts. Remund et al. (2008) evaluated different NWP-based global irradiance forecasts in the USA, reporting relative RMSE values ranging from 20 to 40 % for a 24 h forecast horizon. Similar results were reported by Perez et al. (2009), evaluating NWP-based irradiance forecasts in several places in the USA.

Regarding the forecasts of direct-normal solar irradiance, an additional problem comes into the scene, since direct solar irradiance is not provided by NWP models. Consequently, an additional processing procedure is needed, such as those proposed by Breitkreuz et al. (2009) and Ruiz-Arias et al. (2010). Breitkreuz et al. (2009) proposed a model (called AFSOL) based on the combined use of information provided by a NWP model, an air-quality model and remote sensing retrievals. Ruiz-Arias et al. (2010) propose a new regressive model for the estimation of the hourly diffuse solar irradiation under all sky conditions. The model is based on a sigmoid function and uses the clearness index and the optical air mass as predictors. Lara-Fanego et al. (2012) presented a comprehensive evaluation study of the reliability of direct normal and global forecasts based on the WRF mesoscale model.

Wittmann et al. (2008) analyzed the Spanish premium feed-in tariff model in a case study for a solar-thermal power plant in Andalusia, based on direct-normal solar irradiance forecasts provided by the AFSOL model. This system provides two options for the producers: either transfer the yield to the power distribution company with the electricity sale price stated as a single regulated tariff (tariff model), or sell on the free market at the going market price plus a premium (premium model), which, for solar electricity, is set at 250 % of its average electricity tariff. Operators of installations are obliged to provide the distributor with a forecast of the electricity they intend to feed into the grid the next day by at least 11:00 h (local time) of the previous day. Penalties are established for deviations: the cost of deviation is 10 % of the spot market prices applied to the forecast deviations when the permitted tolerance (20 % for solar and wind power) is exceeded. Interestingly, results proved that the economical benefits that can be achieved based on these forecasts are strongly depended on the time of the day at which forecast deviations take place.

Currently, operational weather forecast models are used with spatial resolutions of a few kilometers. Major National Weather Services intend to implement models with even higher spatial resolution during the next years. The consequences of such downscaling remain to be investigated. At present time, one major short coming is the accurate prediction of the 3D cloud field which is crucial for a good solar production forecast. Furthermore, the implementation of ad hoc measurement data, especially yielded by remote sensing techniques such as satellites, ceilometers, or LIDAR (Light Detection and Ranging) is expected to provide a large potential to improve the forecasts.

References

ABM (2012) Australian bureau of meteorology. http://www.bom.gov.au/

ARM (2012) Department of energy atmospheric radiation measurement. http://www.arm.gov/

ASRC (2012) Atmospheric sciences research center of the university of albany, USA. http://www.asrc.albany.edu/

Badescu V (2002) A new kind of cloudy sky model to compute instantaneous values of diffuse and global solar irradiance. Theor Appl Climatol 72(127–136):2002

Breitkreuz H, Schroedter-Homscheidt M, Holzer-Popp T, Dech S (2009) Short-range direct and diffuse irradiance forecasts for solar energy applications based on aerosol chemical transport and numerical weather modeling. J Appl Meteorol Climatol 48:1766–1779

BSRN (2012) Baseline surface radiation network. http://www.bsrn.awi.de/

Cano D, Monget JM, Guillard H, Albuisson M, Regas N, Wald L (1986) A method for the determination of the global solar radiation from meteorological satellite data. Sol Energy 37:31–39

CEP (2012) Center for Energy and Processes, Ecole des Mines de Paris/Armines, France. http://www.scep.ensmp.fr/

Coiffier J, Sutcliffe C (2012) Funcamentals of numerical weather prediction. Cambridge University Press, Cambridge

CONFRRM (2012) Cooperative networks for renewable resource measurements. http://rredc.nrel.gov/solar/new_data/confrrm/

Cox JD (2002) Storm watchers, John Wiley & Sons, p. 210

Cros S, Wald L (2003). Survey of the main databases providing solar radiation data at ground level. In: Goossens R.i (ed.) Proceedings of the 23rd EARSeL Annual Symposium Remote Sensing in Transition, Ghent, Belgium, 2–4 June 2003, pp. 491–497

DeltaOHM (2012) Pyranometers, albedometers, net irradiance meter. Manual. http://www.Deltaohm.Com/ Ver2008/Uk/Pyra02.Htm

Diabate L, Demarco H, Michaud-Regas N, Wald L (1988) Estimating incident solar radiation at the surface from images of the eath transmitted by geostationary satellites: the heliosat project. Int J Sol Energy 5:261–278

Fröhlich C (1991) History of solar radiometry and the world radiation reference. Metrologia 28:111–115

GAW (2012) Global atmospheric watch. http://www.wmo.int/pages/prog/arep/gaw/gaw_home_en.html

GEWEX (2012) Global energy and water cycle experiment. http://www.gewex.org/

Grell G, Dudhia J, Stauffer D (1998) A Description of the fifth-generation penn state/NCAR mesoscale model (MM5). NCAR tech. note, NCAR/TN-398 + STR, USA

Gueymard CA (2004) The sun's total and spectral irradiance for solar energy application and solar radiation models. Sol Energy 76:423–453

Gueymard CA, Myers DR (2008) Solar radiation measurement: progress in radiometry for improved modeling. In: Badescu V (ed) Modeling solar radiation at the earth surface. Springer, Berlin

Harper K, Uccellini LW, Kalnay E, Carey K, Morone L (2007) 2007: 50th Anniversary of operational numerical weather prediction. Bull Am Meteorol Soc 88(5):639–650

Heinemann D, Lorenz E, Girodo M (2006) Forecasting of solar radiation. In: Wald L, Suri M, Dunlop ED (eds) Solar energy resource management for electricity generation from local level to global scale. Nova Science Publishers, New York

HelioClim (2012) HelioClim server. Centre Energetique et Procedes of Ecole des Mines de Paris. http://www.helioclim.org/heliosat/index.html

Hukseflux (2012) Radiation measurement sensors. Available online http://www.hukseflux usa.com/radiation-measurement.phpAccessed January 2012

Ineichen P, Perez R (2002) A new airmass independent formulation for the linke turbidity coefficient. Sol Energy 73(3):151–157

Isvoranu D (2011) Internal report for project PN-II-ID-PCE-2011-3-0089: Nowcasting and forecasting of PV power plant operation. Polytechnic University of Bucharest, Romania

Janjai S, Laksanaboonsong J, Nunez M, Thongsathitya A (2005) Development of a method for generating operational solar radiation maps from satellite data for a tropical environment. Sol Energy 78:739–751

Janjai S (2008) Generation of solar radiation maps from long-term satellite data. In: Badescu V (ed) Modeling solar radiation at the earth surface. Springer, Berlin

Janjai S, Deeyai P (2009) Comparison of methods for generating typical meteorological year using meteorological data from a tropical environment. Appl Energy 85:528–537

Janjai S (2010) A method for estimating direct normal solar irradiation from satellite data for a tropical environment. Sol Energy 84(9):1685–1695

Kasten F (1980) A simple parameterization of two pyrheliometric formulae for determining the linke turbidity factor. Meteorol Rundsch 33:124–127
Kerr A, Tabony R (2004) Comparison of sunshine recorded by Campbell–Stokes and automatic sensors. Weather 59:90–95
Lara-Fanego V, Ruiz-Arias JA, Pozo-Vazquez D, Santos-Alamillos FJ, Tovar-Pescador J (2012) Evaluation of the WRF model solar irradiance forecasts in Andalusia (southern Spain). Sol Energy. doi:10.1016/j.solener.2011.02.014
Lorenz E, Remund J, Muller SC, Traunmuller W, Steinmaurer G, Pozo D, Ruiz-Arias JA, Fanego VL, Ramirez L, Romeo MG, Kurz C, Pomares LM, Guerrero CG (2009a) Benchmarking of different approaches to forecast solar irradiance. In: 24th European Photovoltaic Solar Energy Conference, Hamburg, Germany, pp. 21–25
Lorenz E, Hurka J, Heinemann D, Beyer HG (2009b) Irradiance forecasting for the power prediction of grid-connected photovoltaic systems. IEEE J Sel Top Appl Earth Obs Remote Sens 2(1):2–10
Lynch P (2008) The origins of computer weather prediction and climate modeling. J Comput Phys 227(7):3431–3444
Martins FR, Pereira EB, Abreu SL (2007) Satellite-derived solar resource maps for Brazil under SWERA project. Sol Energy 81:517–528
Matsangouras IT, Nastos PT, Pytharoulis I (2011) Synoptic-mesoscale analysis and numerical modeling of a tornado event on 12 February 2010 in northern Greece. Adv Sci Res 6:187–194
Mellit A, Pavan AM (2010) A 24 h forecast of solar irradiance using artificial neural network: application for performance prediction of a grid-connected PV plant at trieste. Italy Sol Energy 84(5):807–821
METEONORM (2012) METEONORM software. http://www.meteonorm.com
Molteni F, Buizza R, Palmer TN, Petroliagis T (1996) The ECMWF ensemble prediction system: methodology and validation. Q J R Meteorol Soc 122(529):73–119
Moser W, Rachke E (1984) Incident solar radiation over Europe from METEOSAT data. J Climate Appl Meteorol 23:166–170
Mueller RW, Dagestad KF, Ineichen P, Schroedter-Homscheidt M, Cros S, Dumortier D, Kuhlemann R, Olseth JA, Piernavieja G, Reise C (2004) Rethinking satellite-based solar irradiance modeling: The SOLIS clear-sky module. Remote Sens Environ 91:160–174
NOAA (2008) National oceanic and atmospheric administration. The first climate model http://celebrating200years.noaa.gov/breakthroughs/climate_model/welcome.html
NREL (2012) National renewable energy laboratory. Extraterrestrial solar spectrum. http://rredc.nrel.gov/solar/spectra/am0
Nunez M (1993) The development of a satellite-based insolation model for the tropical western pacific ocean. Int J Climatol 13:607–627
Perez R, Ineichen P, Moore K, Chain C, Kmiecik M, George R, Vignola F (2002) A new operational for satellite-derived irradiances: description and validation. Sol Energy 73(5):307–317
Perez Y, Ramos-Real FJ (2009) The public promotion of wind energy in Spain from the transaction costs perspective 1986–2007. Renew Sust Energ Rev 13(5):1058–1066
Phillips NA (1956) The general circulation of the atmosphere: a numerical experiment. Q J Roy Meteorol Soc 82(352):123–154
Pinker RT, Laszlo I (1992) Modeling surface solar irradiance for satellite applications on the global scale. J Appl Meteorol 24:389–401
PVGIS (2012) Photovoltaic geographical information system. http://re.jrc.ec.europa.eu/pvgis
Reda I (1996) Calibration of a solar absolute cavity radiometer with traceability to the world radiometric reference. Tech. Rep. NREL TP-463-20619, National Renewable Energy Laboratory, Golden, Colorado
Remund Y, Perez R, Lorenz E (2008) Comparison of solar radiation forecasts for the USA. In: 23rd European Photovoltaic Solar Energy Conference, Valencia, Spain, pp. 3141–3143
Rigollier C, Bauer O, Wald L (2000) On the clear-sky models of the ESRA-European radiation atlas, with respect to the heliosat method. Sol Energy 68:33–48

Rigollier C, Lef'evre M, Wald L (2004) The method Heliosat-2 for deriving shortwave solar radiation from satellite images. Sol Energy 77:159–169
Ruiz-Arias JA, Pozo-Vazquez D, Sanchez–Sanchez N, Montavez JP, Hayas-Barru A, Tovar-Pescador J (2008) Evaluation of two MM5-PBL parameterizations for solar radiation and temperature estimation in the south-eastern area of the Iberian peninsula. Il Nuovo Cimento 31(5–6):825–842
Ruiz-Arias JA, Alsamamra H, Tovar-Pescador J, Pozo-Vazquez D (2010) Proposal of a regressive model for the hourly diffuse solar radiation under all sky conditions. Energy Convers Manage 51(5):881–893
Santos-Munoz D, Wolff J, Santos C, García-Moya JA, Nance L (2009) Implementation and validation of WRF model as ensemble member of a probabilistic prediction system over Europe. 10th Annual WRF Users' Workshop, Boulder, USA, 23–26 June 2009
Satel-Light (2012) European database of daylight and solar radiation. http://www.satel-light.com
Schillings C, Mannstein H, Meyer R (2004) Operational method for deriving high resolution direct normal irradiance from satellite data. Sol Energy 76:475–484
Siren KE (1987) The shadow band correction for diffuse irradiation based on a two-component sky radiance model. Sol Energy 39:433–438
SMSE (2012) NASA surface meteorology and solar energy. http://eosweb.larc.nasa.gov/sse/
SRMS (2012) Solar Platform of the West University of Timisoara, Timisoara, Romania. http://solar.physics.uvt.ro/srms
SODA (2012) Solar radiation data. http://www.soda-is.com/eng/index.html
Shuman FG (1989) History of numerical weather prediction at the national meteorological center. Weather Forecast 4(3):286–296
SURFRAD (2012) Surface radiation network, U.S. national oceanic and atmospheric administration. http://www.srrb.noaa.gov/surfrad/index.html
Suri M, Huld T, Dunlop ED (2005) PV-GIS: a web-based solar radiation database for the calculation of PV potential in Europe. Int J Sustain Energ 24:55–67
Suri M, Huld TA, Dunlop ED, Ossenbrink HA (2007) Potential of solar electricity generation in the European Union member states and candidate countries. Solar Energy 81:1295–1305. http://re.jrc.ec.europa.eu/pvgis/
Toth Z, Kalnay E (1997) Ensemble forecasting at NCEP and the breeding method. Mon Weather Rev 125(12):3297–3319
Vonder Haar T, Raschke E, Bandeen W, Pasternak M (1973) Measurements of solar energy reflected by the earth and atmosphere from meteorological satellites. Sol Energy 14:175–184
WCRP (2012) World climate research programme. http://wcrp.wmo.int/wcrp-index.html
Wittmann M, Breitkreuz H, Schroedter-Homscheidt M, Eck M (2008) Case-studies on the use of solar irradiance forecast for optimized operation strategies of solar thermal power plants. IEEE J Sel Top Appl Earth Obs Remote Sens 1(1):18–27
WMO (1983). Report of the meeting of experts on the future activities of the world radiation centre, Leningrad 28 February—1 March 1983. WCP-48, WMO Geneva
WMO (1984). Resolution 6 (EC-XXXVI)—International collection and publication of radiation data. WMO-No.631, Geneva
WMO (2008) Guide to meteorological instruments and methods of observation. world meteorological organization—No. 8 (7th edn.) Chapters 7 and 11
WRDC (2012a). World Radiation Data Center, Main Geophysical Observatory, St. Petersburg, Russia. http://wrdc.mgo.rssi.ru/
WRDC (2012b) World Radiation Data Center, WRDC online archive, National Renewable Energy Laboratory, US Department of Energy. http://wrdc-mgo.nrel.gov/
Zamora RJ, Dutton EG, Trainer M, McKeen SA, Wilczak JM, Hou YT (2005) The accuracy of solar irradiance calculations used in mesoscale numerical weather prediction. Mon Weather Rev 133:783–792
Zelenka A, Perez R, Seals R, Renne D (1999) Effective accuracy of the satellite-derived hourly irradiance. Theor Appl Climatol 62:199–207

http://www.springer.com/978-1-4471-4648-3

Weather Modeling and Forecasting of PV Systems Operation

Paulescu, M.; Paulescu, E.; Gravila, P.; Badescu, V.

2013, XVIII, 358 p., Hardcover
ISBN: 978-1-4471-4648-3